

## Effects of Surface Orientation and Temperature on Tensile Deformation of Gold Nanowires

Qunfeng Liu<sup>1</sup> and Shengping Shen<sup>2</sup>

**Abstract:** Molecular Dynamics (MD) simulations have been performed using the EAM potential to investigate the deformation behaviors and mechanical properties of  $\langle 100 \rangle / \{ 100 \}$  gold nanowires with square cross-section at a certain strain rate under different temperatures ranging from 10 K to 700 K. It is found that  $\langle 100 \rangle / \{ 100 \}$  gold nanowires at high temperatures tend to form the extended stable nanobridges—Helical Multi-shell Structure (HMS), which is similar to the deformation behavior of  $\langle 110 \rangle$  gold nanowires at room temperature reported in the previous experimental observations and simulations. The effect of temperature on the mechanical properties and deformation behaviors of gold nanowires was analyzed. The results showed that the yield stress and modulus of the nanowires with rectangular cross-section decrease with increasing temperature at certain strain rate. In addition, we investigated  $\langle 100 \rangle / \{ 110 \}$  and  $\langle 110 \rangle$  gold nanowires under the same conditions, and found that the surface orientation plays a significant role in the formation and stability of gold nanobridges. Based on these investigations, we discussed the combined effects of surface orientation and temperature on the mechanical properties and structural behaviors. Moreover, the length of HMS and toughness of nanowires with different orientations was analyzed as a function of temperature.

**Keywords:** surface orientation, temperature, tensile deformation, gold nanowires, stable nanobridge.

### 1 Introduction

Nanowires have attracted great interests recently due to their unique structures, properties, and potential applications in nanoelectronicmechanical systems (NEMS) [Kovtyukhova and Mallouk (2002); Lieber (2003); Park and Zimmerman (2005)].

<sup>1</sup> MOE Key Laboratory for Strength and Vibration, School of Aerospace, Xi'an Jiaotong University, Xi'an, Shaanxi 710049, P.R. China.

<sup>2</sup> Corresponding author. MOE Key Laboratory for Strength and Vibration, School of Aerospace, Xi'an Jiaotong University, 28 West Xianning Road, Xi'an, Shaanxi 710049, P.R. China. Tel/Fax: 86-29-82660977; E-mail: sshen@mail.xjtu.edu.cn

The unique properties which are quite different from those of bulk materials are primarily derived from their novel structures with nanometer scale dimension. In the novel structures with nanometer scale dimension, effects of surface confinement are crucial to the unique mechanical, optical, and electrical properties of nanowires. In addition, thermal effect is also a key factor in designing and fabricating nanodevices.

Many experimental works have been performed to reveal the dramatic effects of surface stresses on the mechanical behavior of gold nanowires. For example, some researchers have demonstrated that single-crystal face-centered cubic (fcc) metal nanowires can undergo structural reorientations and phase transformations that are driven by surface stresses [Kondo et al. (1999); Wang et al. (2000)]. Besides structural reorientation and phase transformation, missing-row reconstruction has also been observed on the less unstable higher energy {110} surface of gold nanowires [Wang et al. (2000)]. For the plastic deformation of gold nanowires, the rodlike gold helical multi-shell structures (HMS) with a uniform 3- 4 atoms thickness were observed and the formation of such nanobridges was considered to be stabilized by the hexagonal close-packed (hcp) lattices of the surfaces [Kondo and Takayanagi (1997, 2000); Rodrigues et al. (2000); Oshima et al. (2003)].

Recently, atomistic simulations have been performed to investigate the deformation mechanism of metal nanowires. The novel helical multi-shell structures of metal nanowires have been obtained by some researchers using molecular dynamics [Wang et al. (2001); Park and Zimmerman (2006)]. Park has revealed that the formation of a high strength multi-shell lattice structure during the plastic deformation of the  $\langle 110 \rangle$  wires may account for the stability of the elongated nanobridges observed experimentally [Park and Zimmerman (2006)]. Other mechanical properties, such as lattice reorientation, pseudoelasticity, elastic modulus, yield strength and strain, elastic and plastic deformation of metal nanowires have been studied using molecular simulations as well [Wong et al. (1997); Gall et al. (2004); Liang and Zhou (2005); Wang et al. (2005); Wu et al. (2005)]. All the results demonstrated that the structural and mechanical properties of metal nanowires are closely related to the surface orientation [Park et al. (2006)], loading rate [Ju et al. (2006)], cross-sectional size [Liang et al. (2005)], geometry [Ji and Park (2006)], temperature and so on [Ji and Park (2007); Cao and Ma (2008)].

In this study, we focus on the effects of surface orientation and temperature. The side surface orientation has been certified as the first order effect on the operant mode of inelastic deformation in both  $\langle 100 \rangle$  and  $\langle 110 \rangle$  nanowires [Park et al. (2006)]. Temperature dependence of elasticity modulus and yield stress has been reported for Cu nanopillars with different cross-sectional geometries which is consistent with the experimental observation for bulk Cu [Cao and Ma (2008)].

However, our theoretical knowledge about the combined effects of the surface orientation and temperature on the structural and mechanical properties of metal nanowires is still limited. Most of existed works focus on the elastic deformation behavior under separated effect as mentioned above [Park et al. (2006); Cao and Ma (2008)], and little is known about the systematical post-yield deformation mechanism under the conjunct influence of temperature and surface orientation. In this paper, we investigate the mechanical properties and deformation behaviors of gold nanowires at various temperatures with different surface orientations by means of MD, and study the formation and elongation of HMS. The results are analyzed to discuss the mechanisms of the combined effects of surface orientation and temperature on the mechanical properties and structural behaviors.

## 2 Simulation method

The MD simulations of gold nanowires were conducted using the EAM potential [Daw and Baskes (1984)] as the underlying atomic interaction model. In the EAM, the total energy  $U$  for a system of atoms is written as

$$U = \sum_i^N \left( F_i(\bar{\rho}_i) + \frac{1}{2} \sum_{j \neq i}^N \phi_{ij}(R_{ij}) \right) \quad (1)$$

where the summation in Eq. (1) extend over the total number of atoms  $N$  in the system,  $\phi_{ij}$  is pairwise interaction term which is related to interatomic distance  $R_{ij}$  of atom  $i$  and atom  $j$ ,  $F_i$  is the embedding term which includes the contribution of electron density and provides a many-body contribution,  $\rho_i$  is the electron density at atom  $i$ .

In this work, the EAM potential of Foiles is utilized, which was recently modified to yield an accurate estimation of the intrinsic stacking-fault energy [Park and Zimmerman (2005)], that was critical to the inelastic deformation of gold nanowires.

In the simulations of nanowires, the models were created by ‘top-down’ method from bulk fcc crystal with free boundaries everywhere. The wire was 40 CLU (Cubic Lattice Units) long with rectangular cross-section of 6 CLU  $\times$  6 CLU. To get the equilibrium of the initial models, we used a ‘two-step’ relaxation technique, which consists of the static relaxation and dynamic relaxation. In the first several steps, the whole system was statically relaxed to an equilibrium minimum energy configuration using the conjugated gradient energy minimization. Then the wire was thermally equilibrated to a specific temperature for 10000 ps by means of the Nose-hoover thermostat [Nose (1984); Hoover (1985)] with a time step of 0.01 ps. During the two-step relaxation, the ends of the wires were fixed to keep the length constant.

After the equilibrium was reached, instead of the Nose-hoover thermostat the velocity rescale thermostat would be used, which is readily to ensure an isothermal loading condition during the tensile loading process. One end of the wire kept restrained and the other end free. Then the tensile loading was imposed by applying velocities to atoms along the axial direction that went linearly from zero at fixed end to the maximum value at the free end. It is proved that the loading method employed in the this work is generally independent of the deformation mechanisms and mechanical properties of nanowires [Leach et al. (2007)]. The tensile loading was applied at a two-step constant strain rate at certain temperature. The two-step tensile strain rates were  $3 \times 10^8 \text{s}^{-1}$  for the first 2,000,000 steps and  $1 \times 10^8 \text{s}^{-1}$  for the second 2,000,000 steps respectively. The magnitude of the two strain rates is neither beyond the ability of nowadays' computes, nor too high to affect the thermal properties of the system [Park and Zimmerman (2005)]. The equations of motion were integrated by using velocity-verlet algorithm. All simulations were performed by using LAMMPS [Plimpton (1995); LAMMPS (2008)]. To study the effects of the surface orientation on the deformation of gold nanowires, no periodic boundary conditions were used in this work. In this paper, we only consider the global mechanical behavior of the nanowire, so the average stress and strain of the nanowire are used. Shen and Atluri (2004) proposed an atomic-level stress which is appropriate for both homogeneous and inhomogeneous deformations, while the virial stress [Zhou (2003)] is only appropriate for homogeneous deformation. As discussed in Shen and Atluri (2004), if one averages the proposed atomic-level stress by them over the whole system, the virial stress can be derived. Under homogeneous deformation, both of them are equivalent to the Cauchy stress (Before yielding, the deformation of the nanowire can be assumed to be homogeneous. The elastic modulus are derived from this deformation stage, that is presented in Section 3.3. After yielding, we did not analyze the mechanical behavior quantitatively. Hence, the stress calculation can even be omitted then). So, the average stresses were calculated by using the following formula which can be derived from Shen and Atluri (2004)

$$\sigma_{ij} = \frac{1}{V} \left( \frac{1}{2} \sum_{\alpha=1}^N \sum_{\beta \neq \alpha}^N U' (r^{\alpha\beta}) \frac{\Delta x_i^{\alpha\beta} \Delta x_j^{\alpha\beta}}{r^{\alpha\beta}} \right) \quad (2)$$

where  $N$  is the total number of atoms,  $r^{\alpha\beta}$  is the distance between the two atoms  $\alpha$  and  $\beta$ ,  $\Delta x_i^{\alpha\beta} = x_i^\alpha - x_i^\beta$ ,  $U$  is the potential energy, and  $V$  is the volume of the nanowire. For simplicity, only the average normal stress along the wire axial  $\sigma_{11}$  is considered in these uniaxial tensile loading simulations [Diao et al. (2006)]. The average strain used in this work is defined as the engineering strain which can be written as  $\varepsilon = (l - l_0)/l_0$ , where  $l$  is the current wire length and  $l_0$  is the initial wire length at equilibrium.

### 3 Results and discussion

In this section, a series of MD simulations for  $\langle 100 \rangle / \{100\}$ ,  $\langle 100 \rangle / \{110\}$  and  $\langle 110 \rangle$  gold nanowires are performed at different temperatures ranging from 10K to 700K. The nanowire modes with different orientations are schematically presented in Fig. 1.

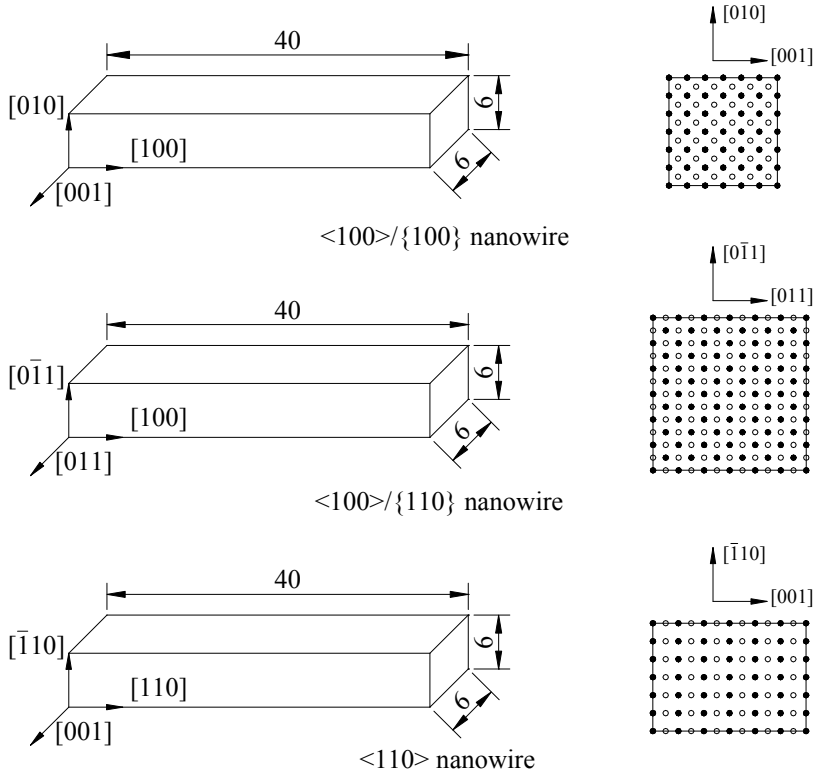


Figure 1: Schematic of nanowire sizes and crystallographic orientations considered in this paper. Transverse atom arrangements are shown to the right of each nanowire. The solid circles and open circles in the cross-sections represent the atoms of the surface layers and the second layers respectively.

#### 3.1 Surface effect

Fig. 2 shows the typical deformation behavior of  $\langle 100 \rangle / \{100\}$  gold nanowire at 10K. Temperature effect is not considered here. The  $\langle 100 \rangle / \{100\}$  gold nanowire

shows full dislocation nucleated from the edge of the wire along a  $\{111\}$  dislocation slip plane when the strain is over the elastic limit, as can be seen in Fig. 2 at  $\epsilon=0.15$ . Once the slip nucleate from the defect of the edge of the wire, high energy side surface  $\{100\}$  will reorient to close-packed and thus lower-energy  $\{111\}$  surface. Soon the wire starts necking in the defect localized region at  $\epsilon=0.30$  leaving the other segment of the wire defect free. With the strain increasing, neck region tends to produce helical multi-shell structure (HMS) and then reorients to stabilized three atom thick chain (ATC) at  $\epsilon=0.37$ . It is well known that the ATC structure is ultra stable in MD simulation, especially at the lower strain rate.

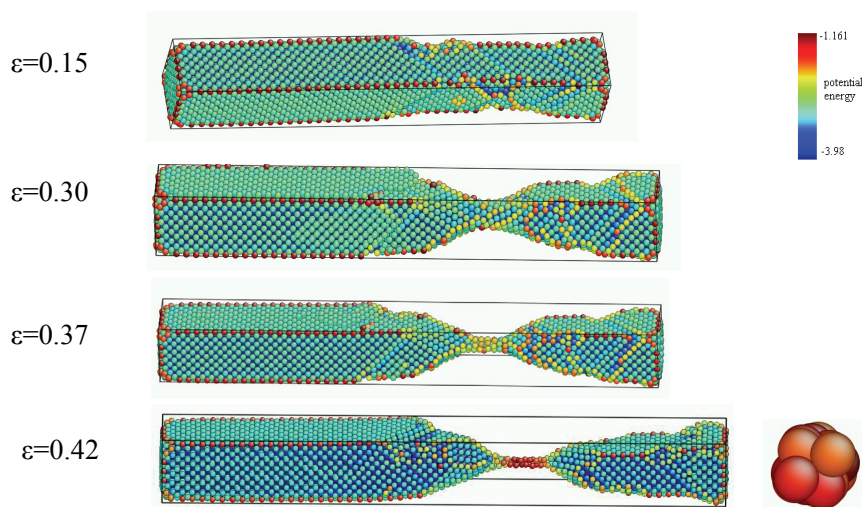


Figure 2: Snapshots of tensile deformation of  $\langle 100 \rangle / \{ 100 \}$  gold nanowire at 10K. The snapshot of the ATC is shown to the right of the corresponding elongated nanowire. Each atom is colored by the value of its potential energy in unit of eV.

The progressive deformation behavior of  $\langle 100 \rangle / \{ 110 \}$  gold nanowires at 10K is shown in Fig. 3. This wire has four less stable higher energy  $\{ 110 \}$  side surfaces. As the  $\{ 110 \}$  surface has higher energy than that of the  $\{ 111 \}$  and  $\{ 100 \}$  facets, surface defects are easily formed under the tensile strain showing missing-row reconstruction and forming irregular ‘saw-tooth’ structures on the  $\{ 110 \}$  side surfaces, as can be seen on the side surface outside the necking region of the wire in Fig. 3 at  $\epsilon=0.15$ . This phenomena is consistent with the experimental observation [Wang et al. (2000)]. The plastic deformation of  $\langle 100 \rangle / \{ 110 \}$  nanowire is characterized by the slip of partial dislocations nucleated from the defects on  $\{ 110 \}$  side

surfaces. With the localization of the initial defects, the wire necks at  $\epsilon=0.32$  and then fractures quickly without the formation of HMS.

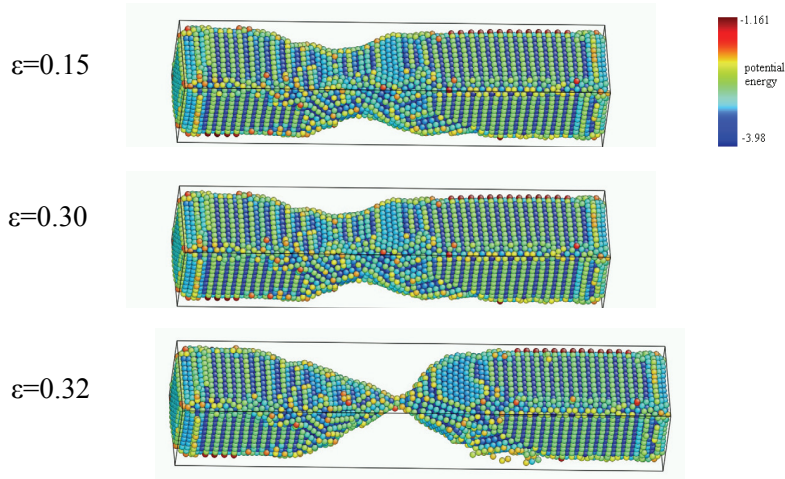


Figure 3: Snapshots of tensile deformation of  $\langle 100 \rangle / \{ 110 \}$  nanowire at 10K. Each atom is colored by the value of its potential energy in unit of eV.

Now, we present the numerical results of  $\langle 110 \rangle$  gold nanowires subjected to the tensile loading at 10K. Snapshots of the deformation process can be seen in Fig. 4.  $\langle 110 \rangle$  nanowire has two  $\{ 110 \}$  side surfaces and two  $\{ 100 \}$  side surfaces. Once the wire yields under tension, the first partial dislocation nucleates from the initial defect on the higher energy  $\{ 110 \}$  surfaces and moves through the cross section along the dislocation glide  $\{ 010 \}$  plane. Next the new partial dislocations are nucleated at the defect line of intersection between the initial dislocation glide plane and the  $\{ 110 \}$  surface forming the  $\{ \bar{1}00 \}$  glide plane. By this way, the dislocations climb zigzag along the whole wire leaving behind several equidistant defect lines on the  $\{ 110 \}$  side surface, as is shown in Fig. 4 at  $\epsilon=0.15$ . With the strain increasing, the inelastic deformation is accommodated firstly by the motion of dislocations and then by the formation of a localized necking [Ji and Park (2007)] at  $\epsilon=0.30$ . In the neck region, the  $\{ 100 \}$  side surfaces reconstruct to form the close-packed amorphous necking surface, while the  $\{ 110 \}$  side surfaces rotate around the defect

line to keep coherency with the neighboring surfaces. When the cross section of necking region is reduced to a few atoms thick, the HMS is formed for several nanometers and then reorients to form the stable ATC structure.

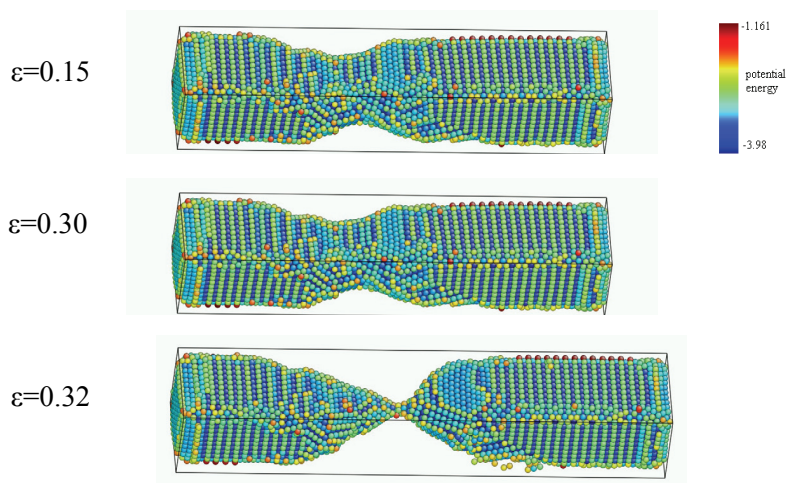


Figure 4: Snapshots of tensile deformation of  $\langle 110 \rangle$  nanowire at 10K. Each atom is colored by the value of its potential energy in unit of eV.

### 3.2 Temperature effect

To investigate the temperature effect on the deformation, the above three kinds of nanowires are simulated at different temperatures. The typical stress-strain curves for  $\langle 100 \rangle / \{ 100 \}$ ,  $\langle 100 \rangle / \{ 110 \}$  and  $\langle 110 \rangle$  nanowires subjected to uniaxial tensile loading at different temperatures are shown in Fig. 5, Fig. 6, and Fig. 7 respectively.

At the first stage of the deformation, the elastic loading process is characterized by monotonically increasing tensile stress with increasing applied strain, followed by a yield point marked by a sudden stress drop [Gall et al. (2004)]. The yield stress can be obtained at the yield point. The elastic modulus is calculated from the linearly fitted initial slope of the stress-strain curve for all the cases. The results show that for each wire at low temperature the deformation mode is necking from the initial defect sites, while at high temperature, increased thermal energy facilitate to activate a large number of defects along the whole wire simultaneously which make the wires more ductile.

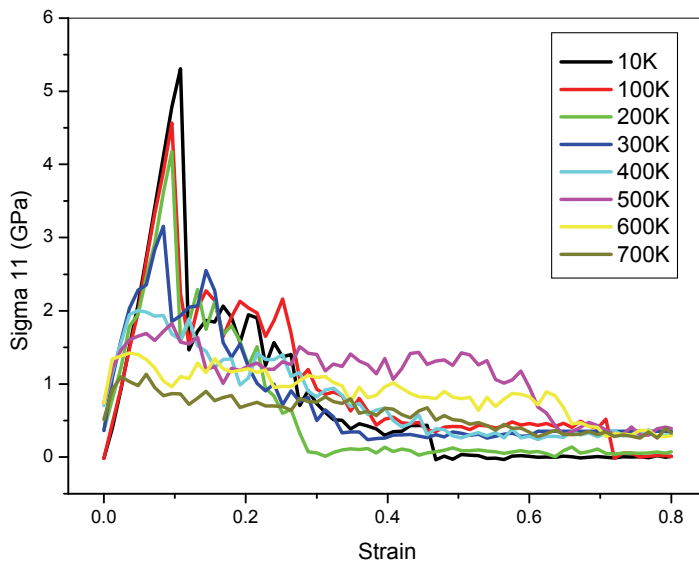


Figure 5: Stress-strain curves for  $\langle 100 \rangle / \{ 100 \}$  nanowire at different temperatures.

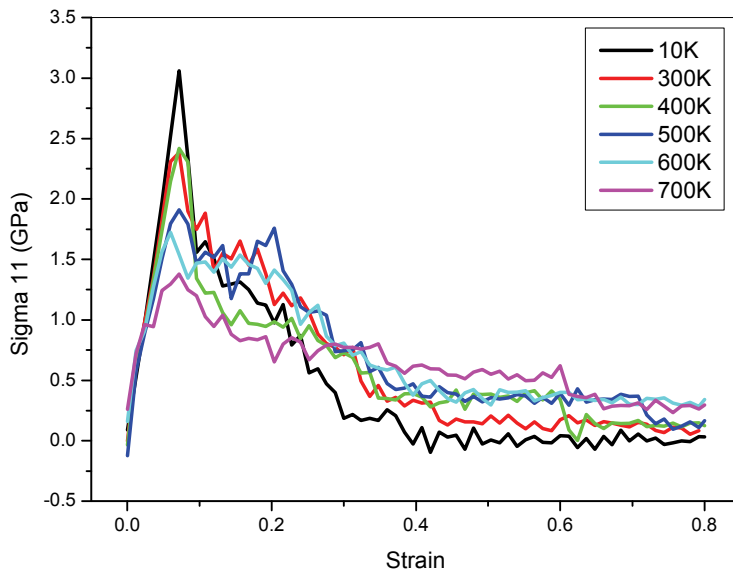


Figure 6: Stress-strain curves for  $\langle 100 \rangle / \{ 110 \}$  nanowire at different temperatures.

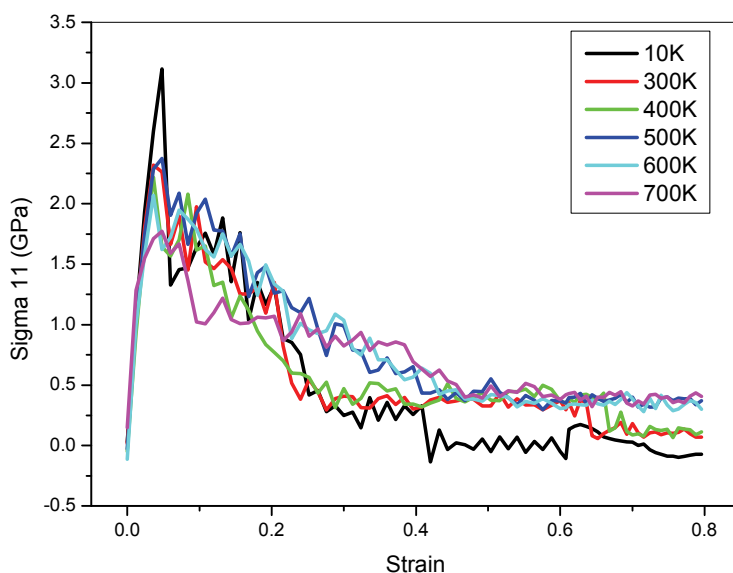


Figure 7: Stress-strain curves for  $\langle 110 \rangle$  nanowire at different temperatures.

### 3.3 Combining effects of surface orientation and temperature

The elastic modulus and yield stress of the three types of gold nanowires are compared at different temperatures, which are illustrated in Fig. 8 and Fig. 9 respectively. For all the three nanowires with different orientations, it is observed that the elastic modulus and yield stress decrease with increasing temperature.

Furthermore, from the yield stress-temperature curves in Fig. 9, the slope of each curve is characterized as the temperature sensitivity of nanowires with a specific surface orientation; qualitatively, the  $\langle 100 \rangle / \{ 100 \}$  wire is more sensitive than the other two wires. This temperature sensitivity disparity occurs for two reasons. First,  $\langle 100 \rangle / \{ 100 \}$  wire has the smallest cross section among the three wires due to its  $\{ 100 \}$  lateral surfaces; smaller wires tend to relax/contract more due to larger surface stresses, so the initial yield stress is higher than the others at low temperatures; however, when the temperature is increased, the thermal effect will be more significant than the other two wires because of the highest ratio of thermal energy to strain energy in  $\langle 100 \rangle / \{ 100 \}$  wire due to its smallest characteristic size.

The second reason is the different deformation mechanism of  $\langle 100 \rangle / \{ 100 \}$  wire from others. Without the influence of thermal energy, the first dislocation usually nucleated at the lateral edges of the  $\langle 100 \rangle / \{ 100 \}$  wire. A higher initial yield stress

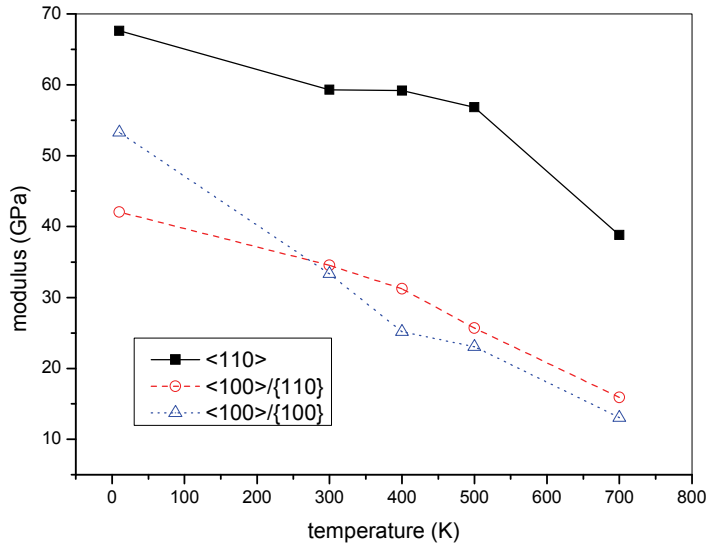


Figure 8: Temperature effect on the modulus of <100>/{100}, <100>/{110} and <110> gold nanowires.

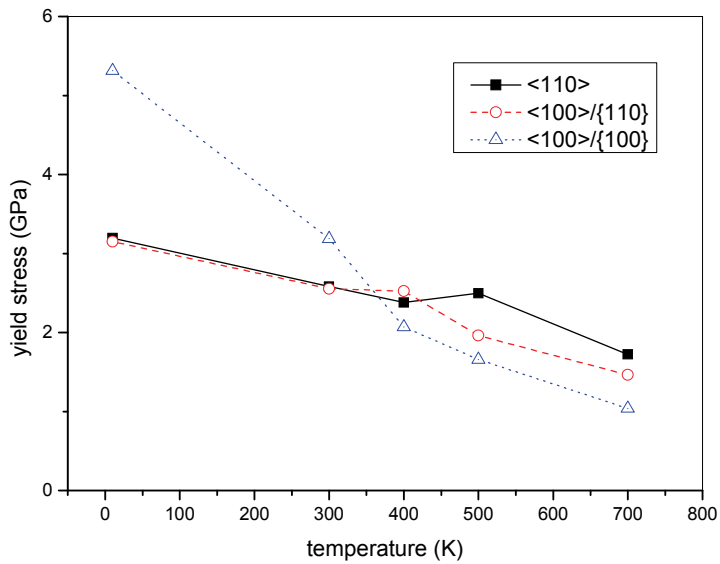


Figure 9: Temperature effect on the yield stress of <100>/{100}, <100>/{110} and <110> gold nanowires.

is needed to drive the first full dislocation to traverse the cross section of the wire along the preferable  $\{111\}$  slip plane. As the temperature increases, the higher thermal energy of the wire will facilitate the nucleation and propagation of partial dislocations which result in the lower yield stress at higher temperatures.

On the other side, it is noted that the modulus of  $\langle 110 \rangle$  wires is significantly larger than that of  $\langle 100 \rangle / \{110\}$  wires at the corresponding temperatures considered. The elastic modulus of metallic nanowires has been investigated by simulations and experiments [Liang et al. (2005); Jing et al. (2006); McDowell et al. (2008a, b)]. All the results showed that the side surface structure and cross-sectional geometry do not significantly affect the modulus of metal nanowires which is strongly dependent on axial orientation. From the results shown in Fig. 8, we find the modulus decreases by 48% averagely between the two types of wires at the same temperature. Another finding is that the modulus decreases by 43% and 62% for  $\langle 110 \rangle$  and  $\langle 100 \rangle / \{110\}$  wire respectively over the temperature range between 10 K and 700 K. That is to say, the modulus of gold wires is strongly dependent on the temperature as well as the axial orientation.

In this work, we also found that the HMS is formed stably with a high strength in some cases [Gall et al. (2004)]. To examine the surface effect and temperature effect on the stability of the HMS, we analyze the deformation processes with the same size and same loading strain rate. The lengths of HMS prior to ATC as a function of the temperature are summarized in Fig. 10 and the typical snapshot of HMS is shown in Fig. 11. As can be seen, the HMS lengths of  $\langle 100 \rangle / \{100\}$  and  $\langle 110 \rangle$  nanowires increase with increasing temperature from 10 K to 500 K and then decrease with increasing temperature from 500 K to 700 K. Again, it is shown that the HMS of  $\langle 100 \rangle / \{100\}$  wires are slightly longer than that of  $\langle 110 \rangle$  wires at the same temperature. Note that the  $\langle 100 \rangle / \{110\}$  wire could not form the HMS until the temperature reaches 400 K and then the HMS length increases with the temperature increasing. This is because the initial defect localization is attributed to the surface effect of  $\{110\}$  side surface of  $\langle 100 \rangle / \{110\}$  wire, which prefer to necking beyond the elastic limit at low temperature. While at higher temperatures, the  $\langle 100 \rangle / \{110\}$  wire is possessed of higher thermal energy. The formation of HMS of the wire at high temperatures is expected to be due to that the combination of thermal energy and tensile strain energy in the necking region facilitate the surface reconstruction which are unfavorable at low temperatures.

The fracture strain of a nanowire under tensile loading is commonly measured at the breaking point to characterize the capacity of sustaining deformation. But in this work, providing the low strain rate, the ATC structure will appear before breaking for all nanowires. Due to the low strength of ATC structure, we define the strain when the ATC structure is formed as the fracture strain  $\varepsilon_f$ . The toughness  $\mu_f$  is then

defined as the strain energy density of the gold nanowires at the ATC formation point [Ji and Park (2007)]:

$$\mu_f = \int_0^{\varepsilon_f} \sigma d\varepsilon, \tag{3}$$

where  $\varepsilon_f$  is the fracture strain and  $\sigma$  is the uniaxial tensile stress. The unit of toughness is  $\text{GJ m}^{-3}$  for all the nanowires in this paper.

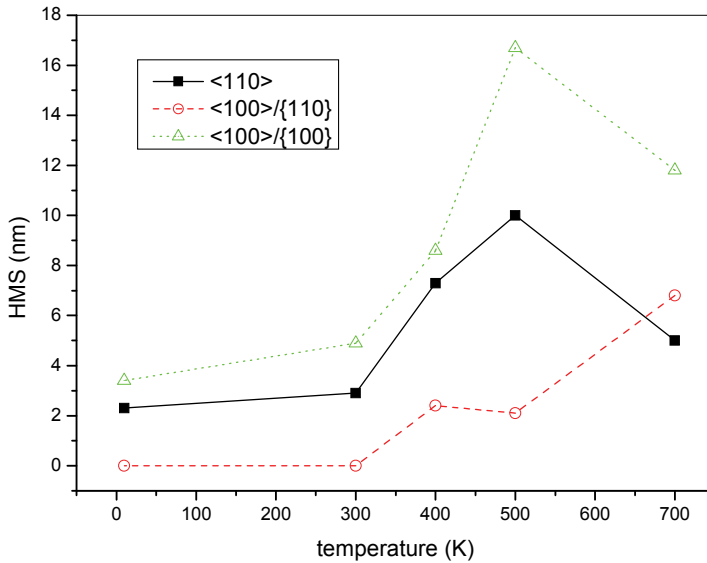


Figure 10: HMS length versus temperature for <100>/100, <100>/110 and <110> gold nanowires.

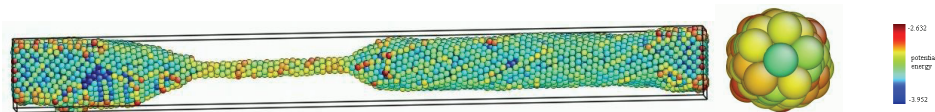


Figure 11: HMS length for <100>/{100} at 500 K. The cross-sectional snapshot of the HMS is shown below the elongated nanowire. Each atom is colored by the value of its potential energy.

As is shown in Fig. 12, it is difficult to ascertain a consistent trend in the toughness of the three types of nanowires over the temperatures ranging from 10 K to 700 K, as there appears to be no correlation between the toughness and the temperature. The only common character of these three curves is that they all get to the maximum toughness at 500 K and then drop down which is similar to the previously mentioned HMS length curve. Interestingly, we found that the toughness of the thinnest  $\langle 100 \rangle / \{ 100 \}$  wire is significantly larger than the other two wires over the temperatures from 10 K to 500 K. As the temperature reaches 700 K, which is close to the melt temperature of gold nanowires, the toughness of  $\langle 100 \rangle / \{ 100 \}$  wire drops sharply to be the smallest one. This phenomenon is related to the strong thermal sensitivity of  $\langle 100 \rangle / \{ 100 \}$  wire discussed in the previous section.

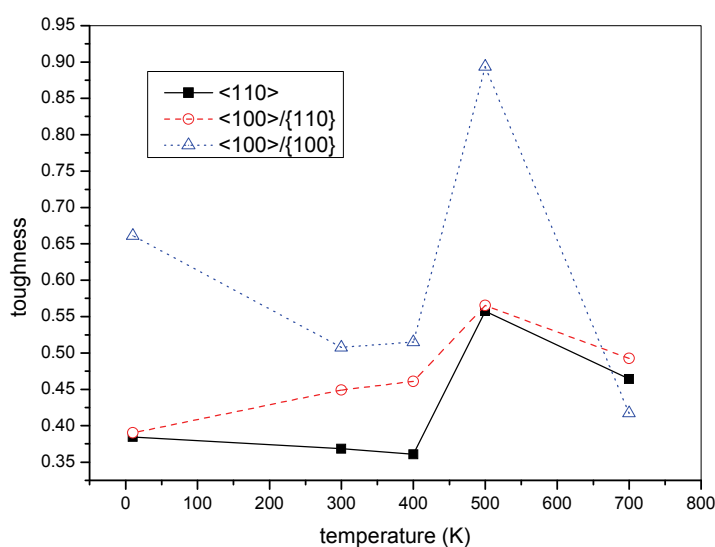


Figure 12: Toughness versus temperature for  $\langle 100 \rangle / \{ 100 \}$ ,  $\langle 100 \rangle / \{ 110 \}$  and  $\langle 110 \rangle$  gold nanowires.

#### 4 Conclusions

In this paper, we first demonstrated how the surface orientation influences the mechanical properties and deformation behaviors of gold nanowires. It is also observed that the yield stress and elastic modulus of the wires with rectangular cross-section decrease with increasing temperatures at a certain strain rate despite surface orientations. Furthermore, the combining effects of surface orientation and tem-

perature on elastic modulus and yield stress are analyzed. The variation of HMS length with increasing temperature is studied for the nanowires with different surface orientations. The toughness is also shown as a function of temperature, and the variation trend of the toughness is to some extent in agreement with that of length of HMS.

**Acknowledgement:** We would like to thank Dr. Harold S Park for his kind help with the use of EAM potential of Foiles. The supports from 973 Program (2007CB707702), NSFC (Grants No. 10672130, 10972173), and Ministry of Education of China are also appreciated.

## References

- Cao, A.; Ma, E.** (2008): Sample shape and temperature strongly influence the yield strength of metallic nanopillars. *Acta Materialia*, 56(17), 4816-4828.
- Daw, M. S.; Baskes, M. I.** (1984): Embedded-atom method: Derivation and application to impurities, surfaces, and other defects in metals. *Physical Review B*, 29(12), 6443-6453.
- Diao, J.; Gall, K.; Dunn, M. L.; Zimmerman, J. A.** (2006): Atomistic simulations of the yielding of gold nanowires. *Acta Materialia*, 54(3), 643-653.
- Gall, K.; Diao, J.; Dunn, M. L.** (2004): The Strength of Gold Nanowires. *Nano Letters*, 4(12), 2431-2436.
- Hoover, W. G.** (1985): Canonical dynamics: Equilibrium phase-space distributions. *Physical Review A*, 31(3), 1695-1697.
- Ji, C.; Park, H. S.** (2006): Geometric effects on the inelastic deformation of metal nanowires. *Applied Physics Letters*, 89(18), 181916-181913.
- Ji, C.; Park, H. S.** (2007): The coupled effects of geometry and surface orientation on the mechanical properties of metal nanowires. *Nanotechnology*, 18(30), 305704-305711.
- Jing, G. Y.; Duan, H. L.; Sun, X. M.; Zhang, Z. S.; Xu, J.; Li, Y. D.; Wang, J. X.; Yu, D. P.** (2006): Surface effects on elastic properties of silver nanowires: Contact atomic-force microscopy. *Physical Review B* 73(23), 235409-235406.
- Ju, S.; Lee, W.; Lin, J.; Liao, M.** (2006): Strain rate effect on tensile behavior of the helical multi-shell gold nanowires. *Materials Chemistry and Physics*, 100(1), 48-53.
- Kondo, Y.; Ru, Q.; Takayanagi, K.** (1999): Thickness Induced Structural Phase Transition of Gold Nanofilm. *Physical Review Letters*, 82(4), 751-754.
- Kondo, Y.; Takayanagi, K.** (1997): Gold Nanobridge Stabilized by Surface Struc-

ture. *Physical Review Letter*, 79(18), 3455-3458.

**Kondo, Y.; Takayanagi, K.** (2000): Synthesis and Characterization of Helical Multi-Shell Gold Nanowires. *Science*, 289(5479), 606-608.

**Kovtyukhova, N. I.; Mallouk, T. E.** (2002): Nanowires as Building Blocks for Self-Assembling Logic and Memory Circuits. *Chemistry - A European Journal*, 8(19), 4354-4363.

**LAMMPS** (2008): <http://lammps.sandia.gov/>.

**Leach, A. M.; McDowell, M.; Gall, K.** (2007): Deformation of Top-Down and Bottom-Up Silver Nanowires. *Advanced Functional Materials*, 17(1), 43-53.

**Liang, H.; Upmanyu, M.; Huang, H.** (2005): Size-dependent elasticity of nanowires: Nonlinear effects. *Physical Review B*, 71(24), 241403-241406(R).

**Liang, W.; Zhou, M.** (2005): Pseudoelasticity of Single Crystalline Cu Nanowires Through Reversible Lattice Reorientations. *Journal of Engineering Materials and Technology*, 127(4), 423-433.

**Lieber, C. M.** (2003): Nanoscale Science and Technology: Building a Big Future from Small Things. *MRS Bulletin*, 28(7), 486-491.

**McDowell, M. T.; Leach, A. M.; Gall, K.** (2008a): Bending and tensile deformation of metallic nanowires. *Modelling and Simulation in Materials Science and Engineering*, 16(4), 045003-045015.

**McDowell, M. T.; Leach, A. M.; Gall, K.** (2008b): On The Elastic Modulus of Metallic Nanowires. *Nano Letters*, 8(11), 3613-3618.

**Nose, S.** (1984): A unified formulation of the constant temperature molecular dynamics methods. *The Journal of Chemical Physics*, 81(1), 511-519.

**Oshima, Y.; Kondo, Y.; Takayanagi, K.** (2003): High-resolution ultrahigh-vacuum electron microscopy of helical gold nanowires: junction and thinning process. *Journal of Election Microscopy*, 52(1), 49-55.

**Park, H. S.; Gall, K.; Zimmerman, J. A.** (2006): Deformation of FCC nanowires by twinning and slip. *Journal of the Mechanics and Physics of Solids*, 54(9), 1862-1881.

**Park, H. S.; Zimmerman, J. A.** (2005): Modeling inelasticity and failure in gold nanowires. *Physical Review B*, 72(5), 054106-054114.

**Park, H. S.; Zimmerman, J. A.** (2006): Stable nanobridge formation in  $\langle 110 \rangle$  gold nanowires under tensile deformation. *Scripta Materialia*, 54(6), 1127-1132.

**Plimpton, S.** (1995): Fast Parallel Algorithms for Short-Range Molecular Dynamics. *Journal of Computational Physics*, 117(1), 1-19.

**Rodrigues, V.; Fuhrer, T.; Ugarte, D.** (2000): Signature of Atomic Structure in

the Quantum Conductance of Gold Nanowires. *Physical Review Letters*, 85(19), 4124-4127.

**Shen, S.; Atluri, S.N.** (2004): Atomic-level stress calculation and continuum-molecular system equivalence. *CMES: Computer Modelling in Engineering & Sciences*, 6: 91-104.

**Wang, B.; Shi, D.; Jia, J.; Wang, G.; Chen, X.; Zhao, J.** (2005): Elastic and plastic deformations of nickel nanowires under uniaxial compression. *Physica E*, 30(1-2), 45-50.

**Wang, B.; Yin, S.; Wang, G.; Buldum, A.; Zhao, J.** (2001): Novel Structures and Properties of Gold Nanowires. *Physical Review Letters*, 86(10), 2046-2049.

**Wang, Z. L.; Gao, R. P.; Nikoobakht, B.; El-Sayed, M. A.** (2000): Surface Reconstruction of the Unstable {110} Surface in Gold Nanorods. *The Journal of Physical Chemistry B*, 104(23), 5417-5420.

**Wong, E. W.; Sheehan, P. E.; Lieber, C. M.** (1997): Nanobeam Mechanics: Elasticity, Strength, and Toughness of Nanorods and Nanotubes. *Science*, 277(5334), 1971-1975.

**Wu, B.; Heidelberg, A.; Boland, J. J.** (2005): Mechanical properties of ultrahigh-strength gold nanowires. *Nat Mater*, 4(7), 525-529.

**Zhou, M.** (2003): A new look at the atomic level virial stress: on continuum-molecular system equivalence. *Proceedings of the Royal Society of London. Series A, Mathematical and Physical Sciences*, 459, 2347-2392.

